INTERNATIONAL JOURNAL FOR NUMERICAL METHODS IN FLUIDS
Int. J. Numer. Meth. Fluids 2008; **56**:739–751
Published online 4 July 2007 in Wiley InterScience (www.interscience.wiley.com). DOI: 10.1002/fld.1554

Development of an electro-osmotic flow model to study the dynamic behaviour in human meridian

Tony W. H. Sheu*, †, Vincent C. Huang and H. P. Rani

Department of Engineering Sciences and Ocean Engineering, National Taiwan University, Taipei, Taiwan

SUMMARY

A numerical study has been performed on the proposed bio-fluid dynamics model to explore and provide some human meridian characteristics. The proposed meridian model involves tissue fluids, which contain ions and nutrition, in the meridian passage. The tissue fluid under investigation can interact with the blood in the capillary vessel at the acupuncture points through a complex electro-osmosis transport process occurring in the meridian path. The investigated physical domain consists of a meridian path having three acupuncture points, namely, gall bladder 37, 38, 39, which are connected with their associated small meridian bodies. Based on the proper physiological coefficients, the simulated mean velocity of the tissue fluid has the result of 3.37 cm/min, and is observed to increase and decrease with the hydraulic pressure of the arteriole with the maximum and minimum values of 4.34 and 2.40 cm/min, respectively. Our simulated results are in good agreement with the experimental findings reported in the literature. In the meridian, both blood and tissue fluid flows exhibited complex electro-osmosis nonlinear behaviour. The immediate response due to the externally applied acupuncture is analysed to reveal the elliptic meridian nature, which is intrinsic in the body fluid. The interaction between the body fluid and blood is as the master and mother, and the influence of the blood circulation on the meridian system and *vice versa* are also analysed in detail. Copyright © 2007 John Wiley & Sons, Ltd.

Received 12 January 2007; Revised 4 April 2007; Accepted 22 May 2007

KEY WORDS: meridian model; tissue fluids; acupuncture points; electro-osmosis transport

1. INTRODUCTION

Meridian theory (channels and collaterals, jingluo) is the central foundation of many unconventional medical systems and, hence, has drawn a considerable attention of many investigators [1, 2]. All meridians form an electrical communication network between the organs of the body (from organ to organ). This results in a continuous electrical loop or circuit that interconnects all parts of the body as one magnificent whole. The meridian theory manipulates the physiological regulation and

*Correspondence to: Tony W. H. Sheu, Department of Engineering Sciences and Ocean Engineering, National Taiwan University, Taipei, Taiwan.
†E-mail: twhsheu@ntu.edu.tw

pathological changes of a human body and is, therefore, the focus of diagnosis and treatment of the traditional Chinese medicine in many aspects, especially in relation to the acupuncture [3, 4]. However, the mechanism of this philologically important meridian system and transduction of acupuncture signals still remain unknown. One of the viewpoints is that the appropriate neural pathways can be activated by the needling or electrical simulation at the acupoints [5, 6]. Previous studies from other research groups have confirmed that in both humans and animals, most acupoints correspond to the high electrical conductance and low skin resistance points on the body surface along the meridians [1, 7–10]. It has been well documented that the skin electrical resistance depends on the activity of the sympathetic nervous system. Stimulation of the sympathetic pathways will result in a lower skin resistance level [11, 12].

Electro-acupuncture has long been known to be more effective than manual acupuncture in relieving the pain [5, 13–17]. Voll [18] showed that the electric resistance is small at the acupuncture point. The energy level of each meridian can be, thus, obtained by measuring the electrical resistance at its associated acupuncture points. Chen [19] proposed an electrical model to describe the acupuncture phenomena in association with the meridian. Notwithstanding the lack of details in these studies, the findings were limited by several methodological issues. With regard to the animal studies, issues of the potentially ambiguous translation of intensities (e.g. 20 times muscle contraction threshold), the generalizability of the hypoalgesic effects and the possibility of the confounding effect of stress-induced analgesia restrict the interpretation and extrapolation of findings to human population. Hence, whilst preliminary electro-acupuncture studies and existing evidences for electro-stimulation in the wider sense suggest a difference in hypoalgesic effect between the varying levels of intensity, findings of electro-acupuncture stimulation in human population remain equivocal. Without this fundamental knowledge of the effect of varying levels of intensity of electro-acupuncture on a normal human population, the relationship between the traditional Chinese therapy and the electro-acupuncture in a clinical setting or in future clinical trials will continue to be the subject of empirical selection [20]. Therefore, this study is aimed to enlighten some of the fundamental electro-osmotic flow (EOF) behaviours in human meridian along with the traditional Chinese therapy.

In the present study, attention is focussed on the exploration of EOF behaviour near the three acupuncture points, namely, gall bladder (GB) 37, 38 and 39 as shown in Figure 1(a). The interaction between the tissue fluid and the blood flow is elucidated. The rest of the paper is organized as follows. Section 2 describes the problem along with the assumptions made to construct the electro-osmotic meridian model. The computational method and the validation of the code used to carry out the current simulation are also highlighted in this section. In Section 3 the results obtained from the proposed electro-osmotic model for the understanding of flow behaviour in the meridian and the interaction between the tissue fluid and blood are presented. Finally, in Section 4 a summary of the present study is provided.

2. COMPUTATIONAL DOMAIN AND METHODOLOGY

The GB meridian is the focus of the present study. At the calf section, the amount of capillaries at the GB acupuncture points (GB 37, 38 and 39 shown in Figure 1(a) [21]) is greater in number than those at the other parts of the body [24]. Furthermore, along the meridian the body fluids in the neighbourhood of these special points contain a comparatively larger quantity of ions, namely, Na^+, Ca^{+2}, K^+, Cl^- and Mg^{+2}. According to the acupuncture theory, the meridian paths exist

DOI: 10.1002/fld

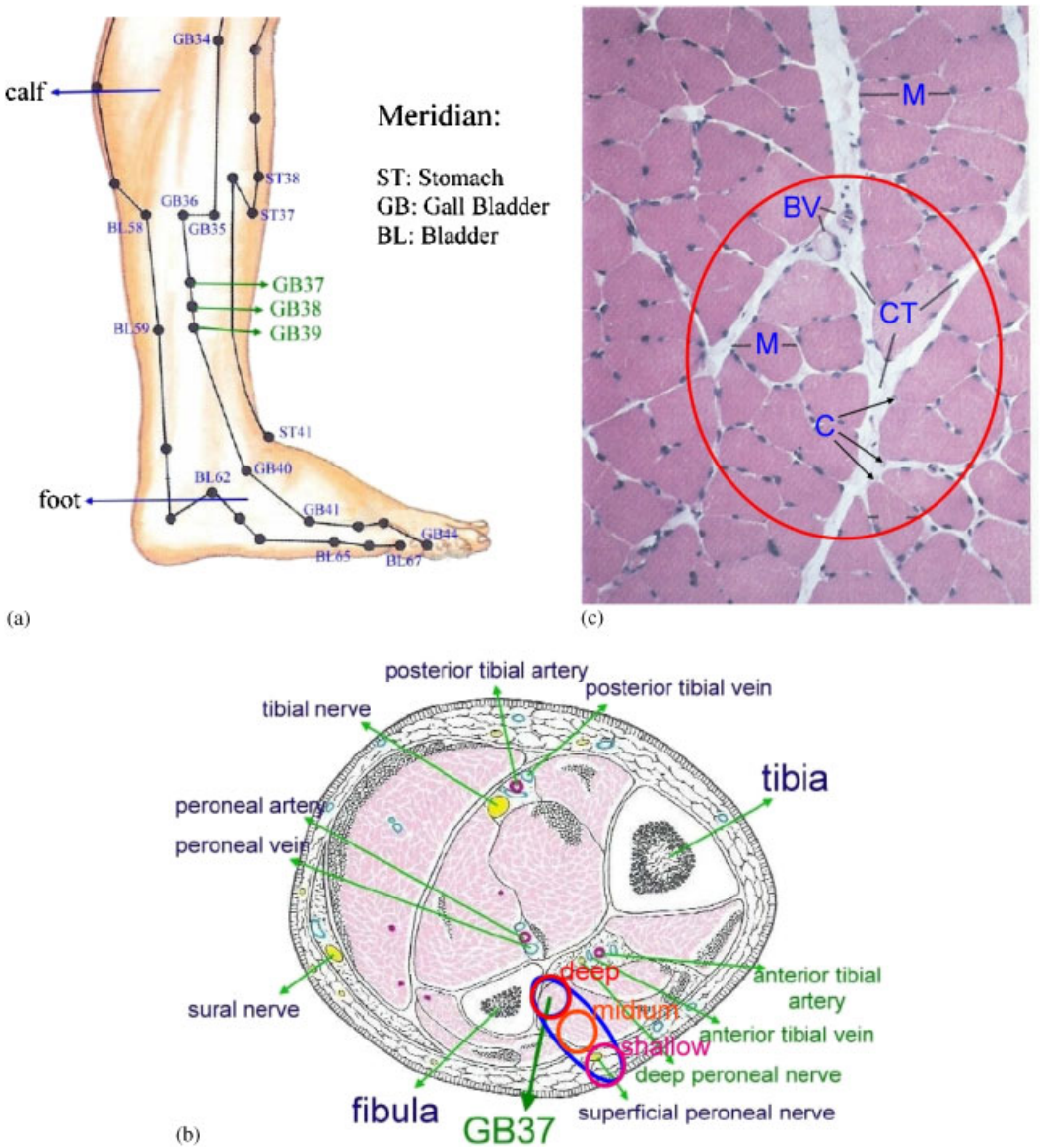

Figure 1. (a) Schematic of the meridian paths of the stomach, gall bladder and bladder. Note that GB37, GB38 and GB39 are the acupuncture points under current investigation [21]; (b) schematic of the axial image of the right leg for the GB37 acupuncture point (Courtesy of Yang [22]); and (c) an axial view of the skeletal muscle (Courtesy of Zhao [23]). The meridian paths existing in the connective tissues, which combine denser capillaries, lymphatic and nerves to form the SMB. (Ps. M, myofibre; BV, blood vessel; CT, connective tissue; C, capillary.)

DOI: 10.1002/fld

between the muscles. It is, therefore, reasonable to consider that Chi is the consequence of the transport of tissue fluids with ions flowing through the gaps of connective tissues of muscles [24–26].

The proposed bio-fluid meridian model is based on the following scientific evidences presented previously: (1) meridian is a continuous channel with different shapes and is connected with various organs through different meridian systems; (2) acupuncture points are harmonically and properly distributed along the meridian and are connected with the blood circulation system through microcirculation; (3) Chi is the consequence of propagating tissue fluids with ions and nutrition. Energy of this sort can be supplied to the whole human body by way of the meridian paths; (4) Along the meridian path, capillaries are densely distributed at the deep positions of acupuncture points, which are filled with the connective tissues [24], in parallel meridian channels and in myofibres. The deep location of acupoint is shown as the red circle in Figure 1(b) [22]. The relation of capillaries and myofibres in skeletal muscle is shown in Figure 1(c) [23].

As pointed out earlier, the acupuncture points are usually found in the muscle fibers. Chi (tissue fluid) and blood can interact with each other at these acupuncture points through the activities initiated by many small meridian bodies (SMBs), which include the muscle fibres, micro-vessels, lymphatic and nerves. To highlight the dynamical behaviour of SMB, three acupuncture points with their respective SMBs were considered in the present study. Both blood circulation and meridian dynamics can, thus, be taken into account. The proposed meridian-circulation system schematic in Figure 2 is to show the interaction of tissue fluid and blood through three acupoints. The flow in the blood vessel and the electro-osmosis tissue fluid flow in the meridian were both assumed to be incompressible and Newtonian. The EOF equations, expressed in terms of velocity ($\underline{u} = (u, v, w)$) and pressure ($p$), are solved along with the electric field equations for the zeta potential (ς) and the externally applied electric potential (φ). The governing equations for mass (continuity equation)

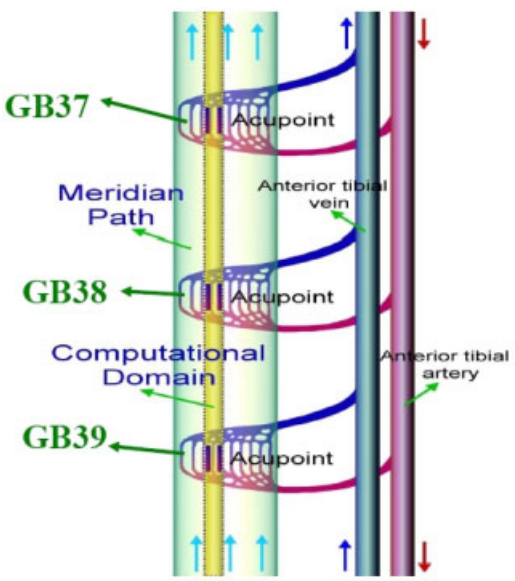

Figure 2. Schematic of the proposed meridian-circulation system.

DOI: 10.1002/fld

and momentum (Navier–Stokes equations) conservations are given by [27]:

$$\nabla \cdot \underline{u} = 0 \tag{1}$$

$$\underline{u} \cdot \nabla \underline{u} + \nabla p - \mu \nabla^2 \underline{u} = \varepsilon \kappa^2 \varsigma \nabla \varphi \tag{2}$$

where $\underline{u}$, μ, κ denote the velocity vector, the dynamic viscosity of the electrolyte solution and the inverse of Debye–Huckel thickness, respectively. The term in the right-hand side of Equation (2) accounts for the formation of an electric double layer and is, therefore, regarded as a good measure of the electro-osmosis force. As the above differential system shows, the electrical potential has to be predicted numerically within a thin electric double layer so as to calculate the source term present in the right-hand side of the momentum equations. In CFD-ACE$^+$ [27], one can choose the embedded electric module to obtain the zeta potential distribution. The Debye–Huckel thickness is prescribed to be the default value 10^{-8} m and griding the electric double layer is not required. As for the electric potential, it was modelled by the following Poisson equation:

$$\nabla^2 \varphi = \frac{F}{\varepsilon_r \varepsilon_0} \sum_{i=1}^{N} z_i c_i \tag{3}$$

where ε_r represents the relative permittivity. It is noted that $\Phi(\equiv \varsigma + \varphi)$ represents the total potential. In the above equation, ε_0, z_i, c_i and F denote the permittivity of the free space, the valence, the concentration and the Faraday constant, respectively. In CFD-ACE$^+$, the right-hand side of Equation (3) is equal to zero for the electro-osmotic problem. To simplify the analysis, the motion of red blood cells and the individual ions is not taken into account. For the modelling of these in the carrier fluid in microcirculation, which can nurture the tissues by the provision of oxygen and nutrient, one can refer to the recently published article [28].

The filtration flow of capillary walls is of the osmotic type in the proposed bio-fluid model. The osmotic velocity depends on the hydraulic and osmotic pressures of the vessels and tissues. According to the Starling equilibrium law [29], the osmotic velocity depends on the hydraulic pressures (blood hydraulic pressure $p^*_{a,v}$ and tissue fluid hydraulic pressure p_0) and osmotic pressures (plasma osmotic pressure π_p and tissue fluid osmotic pressure π_0) of the vessel and tissue. Since there are no coefficients available to represent the osmotic pressures of blood and tissue fluid, the present study considers the simplification given by $p_{a,v} = p^*_{a,v} - \pi_p + \pi_0$. The values of $p^*_{a,v}$, p_0, π_p and π_0 will be given in Section 3 for the current simulation.

Simulation of EOF equations (1)–(3) is carried out by employing the commercially available finite volume package, namely, the CFDRC (CFD Research Corp., Huntsville, AL). The central programs of this software package include the CFD-GEOM for geometry and grid generations, the CFD-ACE$^+$ for flow solver and the CFD-VIEW for post-processing. A convenient graphical user interface is provided for specifying the fluid properties under investigation, boundary and initial conditions. In CFD-ACE$^+$ solver, the finite volume method is employed together with the algebraic multigrid method and conjugate gradient squared solution solver to accelerate the calculation. Also, different orders of upwind schemes can be selected to eliminate the unstable problem due to the convection term shown in Equation (2). The solution procedures are shown in Figure 3.

The geometry of one acupoint physical model employed in the current study is schematically shown in Figure 4(a) and (b). The dimensions and the relationship of the arteriole, venule and lymphatic with the meridian path are clearly depicted in the figures. The lengths and diameters of the capillaries and micro-lymph are specified as 1 mm and 10 μm. The respective wall thickness for

DOI: 10.1002/fld

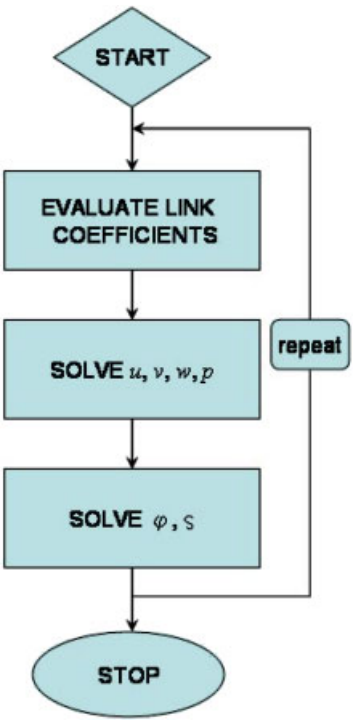

Figure 3. Flowchart of the proposed solution algorithm.

the capillaries and micro-lymph are 1 and 0.5 μm. The distances between acupoints are specified as 20 mm, and the width of meridian path is 0.12 mm. The diameters of the arteriole, venule and lymphatic are all specified as 0.025 mm. Figure 4(c) illustrates the boundary condition, where the pressure and velocity of the arteriole are specified to be larger than the venule, lymphatic vessels and the meridian path. The venule and the lymphatic vessels are prescribed with the negative pressure boundary values, while the median path has the zero pressure boundary value.

In the mesh generation, both structured and unstructured meshes, i.e. hybrid meshes, were employed and are shown in Figure 4(d). There are 654 274 mesh points used to generate the hybrid mesh. The mesh density has been varied so that the computed solutions can achieve the grid independence. In all the investigations, the iterative calculations of primitive variables, such as pressure and velocity, were terminated when the residual norms become less than 10^{-15}. The corresponding residual plot is shown in Figure 5(a). A series of grid-independent tests were conducted to determine the optimal mesh. Figure 5(b) shows the grid-independent results using three mesh densities. From Figure 5(b) it can be observed that when the currently employed mesh points 654 274 were increased by 50% (982 351), the simulated results displayed a negligible variation. On the contrary, when the mesh points were decreased by half (328 673), the variation was evident. Hence, the mesh of nodal points 654 274 is employed in the present simulation. During the simulation, files containing the flow properties were produced. The results were analysed in detail by the plotting and animation tools embedded in the post-processor modules.

DOI: 10.1002/fld

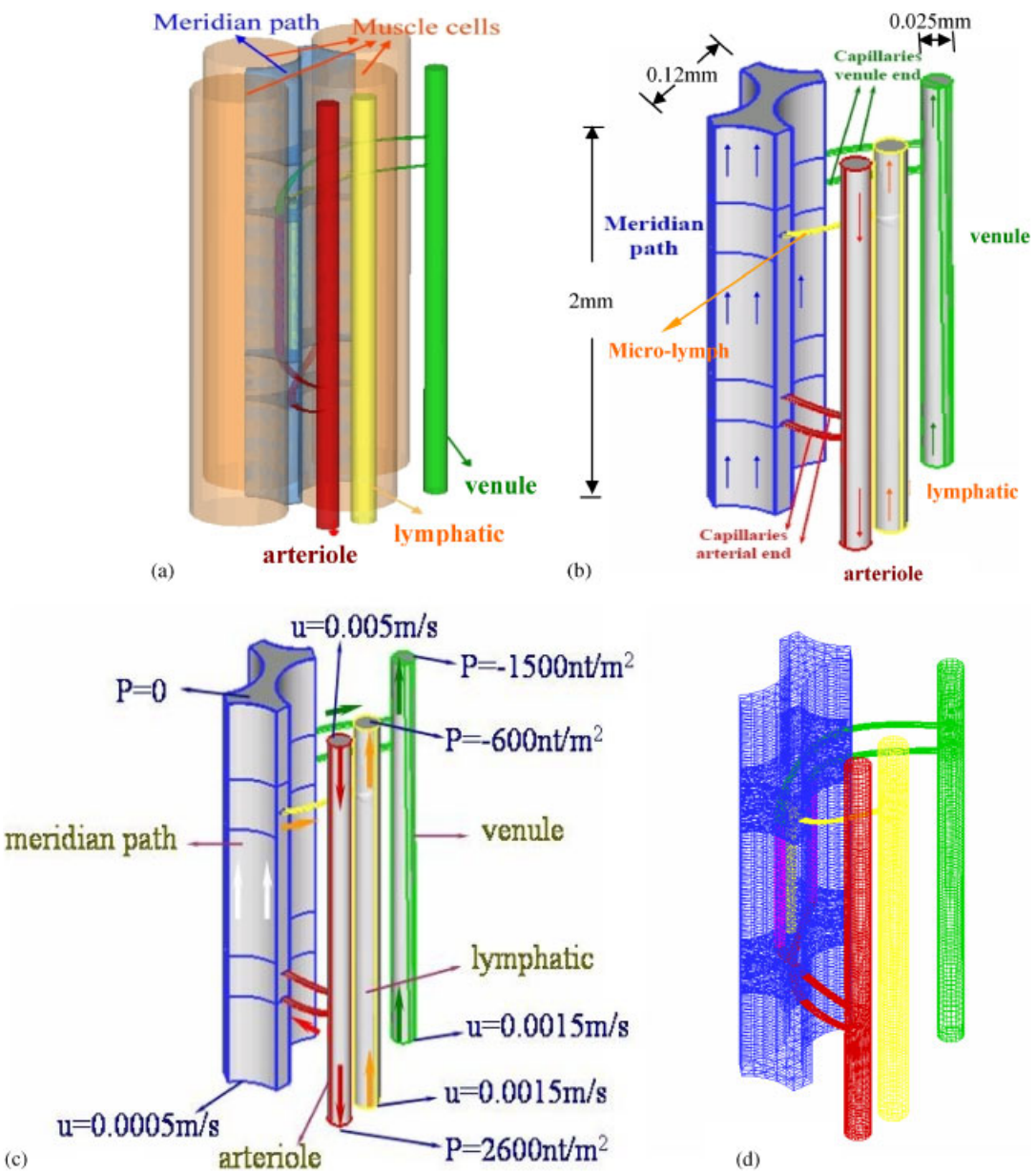

Figure 4. (a) Schematic of the meridian path, arteriole, venule, lymphatic and muscle cell in the proposed model for one representative SMB; (b) schematic of the flow directions for the body fluid and blood in the proposed model given in (a); (c) specified boundary conditions for the proposed 3D numerical model; and (d) representation of the generated meshes in a SMB.

DOI: 10.1002/fld

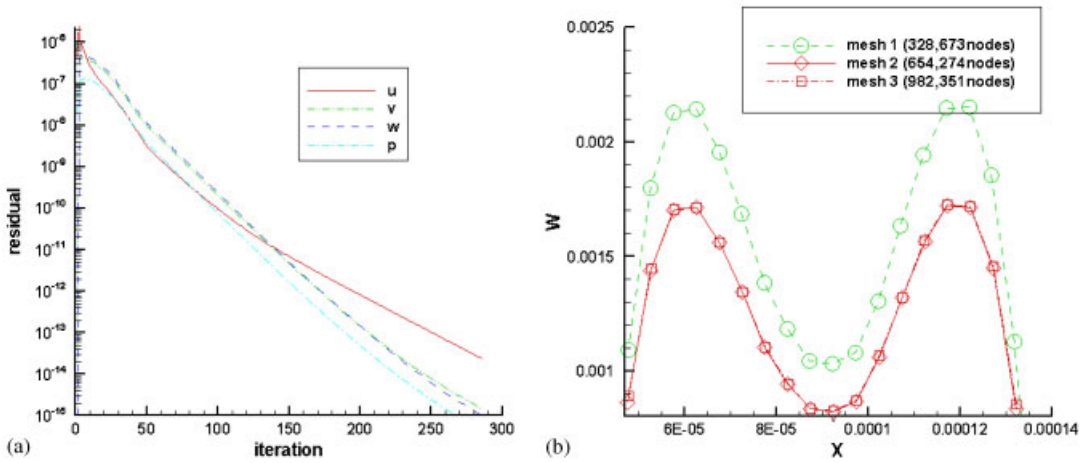

Figure 5. (a) The simulated residual plots and (b) grid-independent test.

3. RESULTS AND DISCUSSION

The mean values of the body fluid and blood velocities in the investigated meridian path and capillaries at the arteriole/venule ends are denoted as u_t ($u_{t\text{-in}}$ and $u_{t\text{-out}}$ were the velocities at the inlet and outlet sides), u_a and u_v, respectively. At the normal state, the hydraulic pressure of the arteriole, venule and tissue were prescribed as $p_a^* = 40$ mmHg, $p_v^* = 10$ mmHg, $p_0 = 0$ mmHg, respectively, and $u_{t\text{-in}}$ was prescribed as $= 3$ cm/min (0.0005 m/s). The osmotic pressures of the plasma and tissue fluids were set as $\pi_p = 25$ mmHg and $\pi_0 = 5$ mmHg, respectively, [30, 31]. In the investigated SMB model, the coefficients are prescribed as $p_a = 20$ mmHg (2666.44 nt/m^2), $p_v = -10$ mmHg (-1333.22 nt/m^2), $p_0 = 0$ mmHg. Along the capillaries and micro-lymph, the porosity (σ) and permeability (k) for vessel's walls were assumed to be 0.0001 and 1.4×10^{-20} m^2, respectively. The kinematic viscosity and density are assumed to be 2.03×10^{-6} m^2/s and 1035 kg/m^3, respectively. The simulated convergent solutions for $u_{t\text{-out}}$, u_a and u_v are 3.37, 105.69 and 97.15 cm/min, respectively. These values are found to have the same orders of magnitude as those in the previous physiological experiments [24–26, 30, 31].

The simulated pressure contours and velocity vector plots are shown in Figure 6(a) and (b), respectively. From Figure 6(a) it is observed that the simulated pressures in the SMB are very high at the arterioles in comparison with the other vessels such as venules and lymphatics. Due to the existence of these pressure gradients between the arterioles and venules, a blood flow proceeding from the arteriole to the venules is resulted. For a pure EOF in the meridian, the electro-kinetic force is balanced by the viscous force and, hence, only small change in the pressure is observed in this region.

The simulated velocity vectors along with the pressure contours inside the meridian depicted in Figure 6(b) highlight the flow nature in the investigated SMB model. For a pure EOF (i.e. without pressure gradient), the predicted velocity is uniform in the bulk of the channel but is sharply varied within the EDL region in order to match the no-slip condition prescribed on the walls. The velocity vectors clearly show that flow enters *via* the arteriole and turns towards the venule (outlet). These

DOI: 10.1002/fld

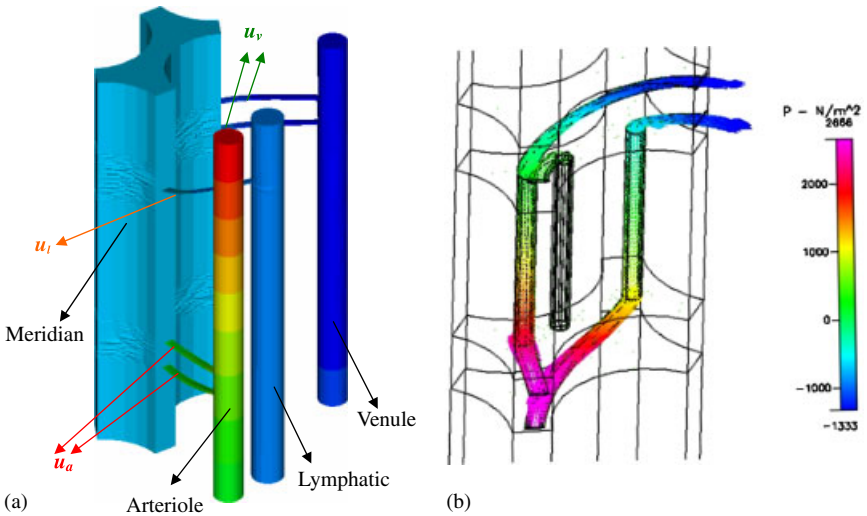

Figure 6. (a) The simulated pressure contours in the SMB and (b) the simulated velocity vectors along with the pressure contours plotted inside the meridian.

Table I. The simulated mean tissue fluid velocities.

	$u_{t\text{-out}}$ (cm/min)	Supporting theory in Chinese medicine
$p_a^* = 30$ mmHg	2.40	Blood is the mother of Chi If blood is weak, then Chi is weak too
$p_a^* = 40$ mmHg	3.37	Normal state
$p_a^* = 50$ mmHg	4.34	If blood is strong, then Chi is strong too

findings are closely agreed with the theoretical results of Overbeek [32], Cummings *et al.* [33] and Santiago [34].

The mutual influence between the blood and body fluid are summarized below according to the simulated results.

Blood is the mother of Chi: Chi present in the tissue fluid exhibits itself as an energy flow due to the existence of ions and nutrition. This specific energy flow stems from the blood system and, hence, the Chinese medicine quotes 'blood is the mother of Chi'. To reveal this important concept scientifically, the blood flow was made to become stronger in the simulated SMB by increasing the hydraulic pressure of arteriole, p_a^*, from 40 to 50 mmHg and the results are tabulated in Table I. It is observed that the velocity of Chi, $u_{t\text{-out}}$, was increased from 3.37 to 4.34 cm/min when the hydraulic pressure of the arteriole is increased. This result implies that when blood becomes strong, Chi also becomes strong. It is also observed that if p_a^* was decreased (from 40 to 30 mmHg) then $u_{t\text{-out}}$ was seen to decrease from 3.37 to 2.40 cm/min. The above result, indicating that when blood pressure becomes weak then Chi becomes weak, coincides with the Chinese medicine quote [35].

Chi blocks and then blood in stasis: In Table II the simulated mean tissue fluid and arteriole velocities are tabulated. It is observed from Table II that when the value of p_0 is altered from 0 to 4

DOI: 10.1002/fld

Table II. The simulated mean tissue fluid velocity and arteriole velocity.

	$u_{t\text{-out}}$ (cm/min)	u_a (cm/min)	Supporting theory in Chinese medicine
$p_0 = 4$ mmHg	2.20	97.56	If Chi is blocked, then blood will be in stasis
$p_0 = 0$ mmHg	3.37	105.69	Normal state
$p_0 = -4$ mmHg	4.54	110.28	If Chi is flowing, then blood is flowing

Table III. Comparison of the simulated mean tissue fluid velocities at the acupuncture and normal states.

k (capillaries) (m^2)	p_a^* (mmHg)	p_v^* (mmHg)	$u_{t\text{-out}}$ (cm/min)	Supporting theory in Chinese medicine
1.4×10^{-20}	40	10	3.37	Normal state
2.8×10^{-20}	50	20	6.04	As tissues are injured by the needles, the response will accelerate the tissue fluid velocity

and -4 mmHg, then $u_{t\text{-out}}$ was predicted to have the values of 2.20 and 4.54 cm/min, respectively. This simulated result reveals that if the hydraulic pressure of tissue fluid is increased, i.e. Chi is blocked, the fluid velocity in the arteriole will be decreased (from 105.69 to 97.56 cm/min) i.e. blood will be in stasis. On the contrary, if the hydraulic pressure of tissue fluids is decreased, i.e. if Chi is flowing, then the fluid velocity in the arteriole will be increased (from 105.69 to 110.28 cm/min) i.e. blood is flowing. According to the Chinese medicine, Chi has the ability to drive the blood flow. From the simulated results and the theory of Chinese medicine, it can be, therefore, inferred that 'if Chi flows, then blood flows too', or 'if Chi blocks, then blood will be in stasis'.

Response of the acupuncture: According to the physiological practice, when the tissue fluids are destructed by an externally applied needle, then the blood is directed to proceed towards the tissue fluids. Therefore, the hydraulic pressure of the capillaries will be increased. Also, the permeability (k) of the resulting capillaries will be increased with the decreasing value of lymphatic. In order to simulate this phenomenon, the permeability value $1.4 \times 10^{-20}\,m^2$ for both vessels and lymphatic was increased to $2.8 \times 10^{-20}\,m^2$ and decreased to $7.0 \times 10^{-21}\,m^2$. According to the simulated results tabulated in Table III, the hydraulic pressures at the arteriole end (p_a^*) and at the venule end (p_v^*) were increased from 40 to 50 mmHg and from 10 to 20 mmHg, respectively. It is observed from the simulated results that the mean tissue fluid velocity $u_{t\text{-out}}$ is increased to 6.04 cm/min. This simulated result implied that the Chi energy has been strengthened when the tissue fluids are destructed by the externally applied pressure.

Electro-acupuncture study: The underlying theory of electro-acupuncture can be explained with the help of the electric wave phenomenon of Chi, since the tissue fluids present in the meridian channel are rich in ions. In the clinical therapy, both the electric paste-piece and electro-acupuncture treatments have been widely employed. To study the electric paste-piece effect, two externally applied potentials of $V_{ext} = 50$ and 0 V were imposed at the inlet of tissue fluids of the first

DOI: 10.1002/fld

Table IV. Comparison of the simulated mean tissue fluid velocities due to the externally applied voltages at the electro-acupuncture and normal states.

	$u_{t\text{-out}}$ (cm/min)	Consequence
Normal state	3.37	
External voltage (electric paste-piece)	3.45	Electric paste-piece can provide an external potential between the inlet and the outlet of the tissue fluid. An electro-osmosis flow is resulted
Electro-acupuncture	6.11	Electro-acupuncture has the better efficacy than the acupuncture or the electric paste-piece

acupuncture point and at the outlet of the tissue fluids of the third acupuncture point, respectively. In Table IV the comparison of the simulated mean tissue fluid velocities due to the external voltages applied at the electro-acupuncture and normal states is shown. It was observed that the resulting tissue fluid velocity was seen to increase from 3.37 to 3.45 cm/min. Also, the electro-acupuncture phenomenon was simulated by taking the hydraulic pressure (p_a^*, p_v^*) and permeability (k) for both vessels and lymphatic into account. The resulting velocity magnitude of $u_{t\text{-out}}$ was observed to be larger (6.11 cm/min) in comparison with the value obtained from the case under the electric paste-piece (3.45 cm/min) treatment.

4. CONCLUDING REMARKS

Our proposed meridian dynamic model is rooted in two elliptic equations, namely, the Poisson equation for the electric potential and the Navier–Stokes equations for the fluid flows. The tissue fluid motion in the investigated model was considered to be of the creeping flow type with the Reynolds number of 0.0286. The blood circulation in the vessel and the body fluid motion in the meridian path are simulated within the complex electro-osmosis dynamical framework. By solving the electric potential equation and the modified Navier–Stokes equations that are applicable to the present bio-fluid system, the simulated electrostatic potential distribution and the blood/tissue fluid velocity profile in response to the applied electric field and/or a pressure gradient are obtained numerically. The dynamic fluid behaviour in the meridian path is found to be similar to the experimental observations reported in the literature in the sense that blood circulation can be affected by the meridian system and *vice versa*. The essences of Chinese medicine, namely, 'blood is Chi's mother', and 'Chi and blood depend on each other' are computationally confirmed through the present study.

ACKNOWLEDGEMENT

The first author would like to thank Prof. Ding Guanghong, who inspired this study in the year 2000 when he was invited to give a talk in the Department of Mechanics and Engineering Science of Fudan University during his sabbatical leave in the Shanghai University.

DOI: 10.1002/fld

REFERENCES

1. Chiou SY, Chao CK, Yang YW. Topography of low skin resistance points (LSRP) in rats. *The American Journal of Chinese Medicine* 1998; **26**:19–27.
2. Zhu ZX, Hao JK. Electric characteristics of the skin along meridian lines. *Acupuncture Meridian Biophysics-Scientific Verification of the First Great Invention of China*. Beijing Press: Beijing, 1989; 189–232.
3. Qian XZ. Progress in scientific research on acupuncture, moxibustion and acupuncture anesthesia by integrating traditional Chinese and Western medicine. *Research on Acupuncture*, *Moxibustion*, *and Acupuncture Anesthesia*. Science Press: Beijing, 1986; 1–18.
4. Tang D. Advances of research on the mechanism of acupuncture and moxibustion. *Acupuncture Research* 1987; **4**:278–284.
5. Ulett GA, Han S, Han JS. Electroacupuncture: mechanisms and clinical applications. *Biological Psychiatry* 1998; **44**:129–138.
6. Zhu B. *Scientific Foundations of Acupuncture and Moxibustion*. Qingdao Press: Qingdao, 1998.
7. Fraden J. Active acupuncture point impedance and potential measurements. *American Journal of Acupuncture* 1979; **7**:137–144.
8. Hu XL, Cheng XN. *Meridian Research* (Chinese National Climbing Project). Hunan Science and Technology Press: Hunan, 1997.
9. Luciani RJ. Direct observation and photography of electroconductive points on human skin. *American Journal of Acupuncture* 1978; **6**:311–317.
10. Reichmanis M, Marino AA, Becker RO. Skin conductance variation at acupuncture loci. *The American Journal of Chinese Medicine* 1976; **4**:69–72.
11. Korr IM, Thomas PE, Wright HM. Patterns of electrical skin resistance in man. *Acta Neurovegetativa* 1958; **17**:77–96.
12. Smith GB, Wilson GR, Curry CH, May SN, Arthurson GM, Robinson DA, Cross GD. Predicting successful brachial plexus block using changes in skin electrical resistance. *British Journal of Anaesthesia* 1988; **60**:703–708.
13. Wan Y, Wilson SG, Han J, Mogil JS. The effect of genotype on sensitivity to electro-acupuncture analgesia. *Pain* 2001; **91**:5–13.
14. Mao W, Ghia JN, Scott DS, Duncan GH, Gregg JM. High versus low intensity acupuncture analgesia for treatment of chronic pain: effects on platelet serotonin. *Pain* 1980; **8**:331–342.
15. Han J, Zhou Z, Xuan Y. Acupuncture has an analgesic effect in rabbits. *Pain* 1983; **15**:83–91.
16. Romita VV, Suk A, Henry JL. Parametric studies on electro-acupuncture-like stimulation in a rat model: effects of intensity, frequency, and duration of stimulation on antinociception. *Brain Research Bulletin* 1997; **42**:289–296.
17. Huang C, Wang Y, Han JS, Wan Y. Characteristics of electroacupuncture-induced analgesia in mice: variation with strain, frequency, intensity, and opioid involvement. *Brain Research* 2002; **945**:20–25.
18. Voll R. The phenomenon of medicine testing in electroacupuncture according to Voll. *American Journal of Acupuncture* 1980; **8**:97–104.
19. Chen KG. Electrical properties of meridians. *IEEE Engineering in Medicine and Biology Society* 1996; **May/June**: 58–63.
20. Barlas P, Ting SLH, Chesterton LS, Jones PW, Sim J. Effects of intensity of electroacupuncture upon experimental pain in healthy human volunteers: a randomized, double-blind, placebo-controlled study. *Pain* 2006; **122**:81–89.
21. Chang KW. *Meridian Anatomy*. Zhi-Yang Press: China, 1999; 47.
22. Yang JK. *Meridian Cross-section Anatomy*. Shang Hai Science Technology Press: China, 1997; 76.
23. Zhao JF. *Color Atlas of Medical Histology*. Yi-Xuan Press: Taipei, 1997.
24. Fei L. Researches and developments of meridian physical basic and function experiments. *Chinese Science Bulletin* 2000; **43**(6):658–672.
25. Tiberiu R, Gheorghe G. Do meridians of acupuncture exist? A radioactive tracer study of the bladder meridian. *American Journal of Acupuncture* 1981; **9**(3):251–256.
26. Darras JC, Vernejoue P. Albarede P. Nuclear medicine and acupuncture: a study on the migration of radioactive tracers after injection at acupoints. *American Journal of Acupuncture* 1992; **20**(3):245–256.
27. *CFD-ACE-GUI User Manual Volume II*. CFD Research Corporation, 2003; 85–94.
28. Cristini V, Kassab GS. Computer modeling of red blood cell rheology in the microcirculation: a brief overview. *Annals of Biomedical Engineering* 2005; **33**(12):1724–1727.
29. Starling EH. On the adsorbtion of fluid from interstitial spaces. *The Journal of Physiology* 1896; **19**:312–326.
30. Guyton AC. *Textbook of Medical Physiology* (10th edn). WB Saunders: Philadelphia, 2000.
31. Valtin H, Schafer JA. *Renal Function* (3rd edn). Little-Brown: Boston, 1995.

DOI: 10.1002/fld

32. Overbeek JTG. Stability of hydrophobic colloids and emulsions. In *Colloid Science*, Kruyt HR (ed.), vol. 1. Elsevier: Amsterdam, 1952; 302–341.
33. Cummings EB, Griffiths SK, Nilson RH, Paul PH. Conditions for similitude between the fluid velocity and electric field in electroosmotic flow. *Analytical Chemistry* 2000; **72**:2526–2532.
34. Santiago J. Electroosmotic flows in microchannels with finite inertial and pressure forces. *Analytical Chemistry* 2001; **73**:2353–2365.
35. Maoshing Ni (translator). *The Yellow Emperor's Classic of Medicine*: *A New Translation of the Neijing Suwen with Commentary*. Shambhala: Boston, 1995.

DOI: 10.1002/fld